Journal of ELECTRONIC MATERIALS, Vol. 47, No. 11, 2018
https://doi.org/10.1007/s11664-018-6552-7


# Effect of Praseodymium Doping on Structural and Electrochemical Performance of Lithium Titanate Oxide ($Li_4Ti_5O_{12}$) as New Anode Material for Lithium-Sulfur Batteries

MOHAMMAD REZA SOVIZI [1,3] and SEYEDEH MASOOMEH POURALI[2,4]

1.—Department of Chemistry, Malek Ashtar University of Technology, P.O. Box 16765-3454, Tehran, Iran. 2.—Department of Chemical Engineering, Biofuel and Renewable Energy Research Center, Babol Noshirvani University of Technology, P.O. Box 47148-71167, Babol, Iran. 3.—e-mail: mrsovizi@mut.ac.ir. 4.—e-mail: pourali.masoomeh@yahoo.com

In spite of their high theoretical energy density and potentially low cost, lithium-sulfur batteries face several challenges in their path toward widespread adoption, among which introduction of an appropriate anode seems to be one of the most difficult. We report herein on a modified anode based on lithium titanate oxide ($Li_4Ti_5O_{12}$) (LTO) doped with praseodymium (Pr) element. A fairly simple sol–gel procedure was employed to prepare praseodymium-doped lithium titanate oxide (Pr-LTO). Different techniques were then applied for structural and morphological characterization of LTO and Pr-LTO, including x-ray diffraction analysis, Brunauer–Emmett–Teller surface area measurements, and scanning electron microscopy. Although the LTO and Pr-LTO electrodes were prepared using similar procedures, the Pr-LTO electrode exhibited higher capacity as well as better cycling efficiency compared with LTO. The Pr-LTO electrode demonstrated high rate capability along with reversible capacity of 173 mAh $g^{-1}$, 116 mAh $g^{-1}$, and 62 mAh $g^{-1}$ at 0.05 C, 1 C, and 2 C, respectively. Electrochemical impedance spectroscopy also confirmed that Pr-LTO had higher electronic conductivity and faster lithium-ion diffusion compared with LTO.

**Key words:** Lithium-sulfur batteries, lithium titanate oxide, praseodymium, doping

## INTRODUCTION

In the future, petroleum-based energy will be limited, so development of alternative, sustainable, and clean energy technologies will be necessary to supply or replace fossil-fuel energy. Solar and wind energy sources are candidates, but their practical application is greatly limited because they are not controllable and suffer from intermittency.[1,2] Secondary batteries, such as lithium-ion batteries (LBs), are an important component of energy storage devices in the field of new energy technologies, owing to their high energy conversion efficiency and energy density.[3] Rechargeable lithium batteries have been used extensively as power sources in various portable electronic devices.[4] Recently, much effort has been dedicated to promoting their applications in hybrid electric vehicles and dispersed energy storage systems, due to their many advantages such as high energy density, small volume, required light weight, and safety.[5,6] Although lithium-ion batteries are one of the best candidates for these fields, their applications are limited for many reasons, including high cost and limited theoretical energy density.[7] To overcome these obstacles, lithium-sulfur (Li-S) batteries are the most promising candidates, due mainly to their high theoretical energy density.[8,9] However, many technical challenges must be faced, including choice of appropriate electrolytes,[10] cathodes,[11,12] and anodes

(Received November 6, 2017; accepted July 25, 2018; published online August 9, 2018)

for Li-S batteries. In these batteries, lithium metal is used as the lithium source (anode). Lithium metal is regarded as a preferred electrode material for the anode of lithium-sulfur batteries, mainly due to its excellent performance in terms of gravimetric density (0.59 g $cm^{-3}$), high theoretical specific capacity (3860 mAh $g^{-1}$), and good negative redox potential (−3.040 V versus standard hydrogen electrode). However, two main problems must be solved before use of such lithium anodes.[13]

One is that lithium metal can easily react with the electrolyte, usually resulting in poor charge–discharge cycling efficiencies due to severe growth of the solid electrolyte interface (SEI) layer.[14] The other problem is formation and growth of lithium dendrites on the lithium anode surface, seriously hindering practical applications of lithium-sulfur batteries.[15]

Several modifications have been proposed to enhance the applications of such batteries, including modification of the surface of the Li anode,[16] deposition of Li with carbon nanospheres,[17] protection of the Li anode via polymerization,[14] application of lithiated silicon instead of Li metal,[18] implementation of silicon-, carbon-,[19,20] and tin-based anodes,[7] Li-B (boron) alloys,[21,22] and hybrid anodes.[23]

Spinel LTO offers many advantages over currently used anodes[24] for application in LIBs; For instance, there is a trivial change in the unit cell volume of LTO during lithium insertion and extraction, making it a zero-strain material.[25] Furthermore, offering a very stable, flat voltage plateau at around 1.55 V versus $Li/Li^+$, which is higher than the reduction potential of most organic electrolytes, LTO is considered to be much safer and more stable than other anode materials such as carbon. Despite these advantages, further applications of LTO face various major challenges. One of the main intrinsic obstacles to development of LTO is its low electronic conductivity, which leads to low rate capacity. To overcome this problem, three methods have been proposed: (1) synthesis and use of nanomaterials, because nano particle size obviously shortens lithium-ion diffusion paths and broadens the electrode–electrolyte contact surface[19,26–28]; (2) addition of a second conductive phase into the LTO, such as metal powder and carbon[29–31]; (3) substitution of Li or Ti by other metal cations, such as $Cr^{3+}$, $V^{5+}$, $Mn^{4+}$, $Fe^{3+}$, $Zr^{+4}$, $Al^{3+}$, $Ga^{3+}$, $Co^{3+}$, $Ta^{5+}$, and $Cu^{2+}$.[32–35]

The aim of this study is to prepare and characterize Pr-LTO as a new anode material for lithium-sulfur batteries. To the best of the authors' knowledge, no investigation has hitherto been conducted on the electrochemical characteristics of Pr-doped LTO as anode material for Li-S batteries. For this work, $Ti^{4+}$ was partially substituted with $Pr^{3+}$, causing a certain amount of $Ti^{4+}$ to change to $Ti^{3+}$ to achieve charge compensation. The transition from $Ti^{4+}$ to $Ti^{3+}$ in LTO leads to an increase in the electronic conductivity and thus improves the electrochemical performance of the electrode, especially its rate capability.

## EXPERIMENTAL PROCEDURES

### Chemicals

Lithium acetate ($CH_3COOLi$), titanium tetraisopropoxide $Ti[OCH(CH_3)_2]_4$, praseodymium nitrate [$Pr(NO_3)_3$], polyvinyl difluoride (PVDF), and *N*-methyl-2-pyrrolidone (NMP) were obtained from Merck (Germany), and lithium sulfide ($Li_2S$), $Li_2S$, lithium bis(trifluoromethanesulfonyl)imide (LiTFSI), polyethylene (Celgard 2400), dimethyl ether (DME), and 1,3-dioxolane (DOL) were all purchased from Sigma–Aldrich (USA). Carbon black (Akzo Nobel) was purchased from Fluka (USA). High-purity water was prepared using a Millipore water purification system (Billerica, MA, USA).

### Apparatus

X-ray diffraction (XRD) patterns were obtained from powders directly using a Bruker diffractometer (AXS, D8) with Cu $K_\alpha$ radiation. Field-emission scanning electron microscopy (FE-SEM) was carried out using a Mira 3-XMU. Specific surface area and nitrogen adsorption–desorption isotherms of the synthesized LTO and Pr-LTO were measured using a BELSORP-miniII (MicrotracBEL, Japan) instrument. Cyclic voltammetry and electrochemical impedance spectrum (ESI) measurements were performed using a VSP 300 (Biologic, France) electrochemical workstation. The capacity, cyclability, and rate capability of the manufactured cells were analyzed based on the charge–discharge characteristics obtained using a battery cycler system (Kimiastat 126, Kimiapardaz Iran, Iran).

### Synthesis of LTO and Pr-LTO

Pr-LTO was synthesized via a sol–gel method,[36] with stoichiometric amounts of lithium acetate ($CH_3COOLi$), titanium tetraisopropoxide $Ti[OCH(CH_3)_2]_4$, and praseodymium nitrate [$Pr(NO_3)_3$] as starting materials. The resulting gel was dried at 100°C for 24 h to evaporate excess ethanol, yielding organic precursors that were then calcined in an oven at 800°C for 12 h to obtain the final powders, whose color was light green in comparison with the white pristine LTO powder prepared using the same procedure. The crystal structure of the powders was characterized by x-ray diffraction analysis. Particle size and morphology were observed by scanning electron microscopy.

### Cell Assembly and Electrochemical Measurements

Electrodes were fabricated by mixing active material [lithium sulfide ($Li_2S$) for cathode, LTO and Pr-LTO for anode], carbon black, and polyvinylidene

fluoride (PVDF) at ratio of 80:10:10 (w/w/w) in *N*-methyl-2-pyrrolidine (NMP) as solvent, to obtain a slurry that was subsequently uniformly coated on a copper current collector and dried at 70°C for 1 h to remove the solvent. The electrode foil was punched into circular discs, which were used to assemble coin cells in an argon-filled glovebox with oxygen and moisture content below 1 ppm. Solution containing 1.0 mol $dm^{-3}$ lithium bis-(trifluoromethanesulfonyl)imide (LiTFSI) in mixed solvent of 1,3-dioxolane (DOL) and 1,2-dimethoxyethane (DME) (1:1, V/V) with addition of 0.5 M $LiNO_3$ was used as electrolyte, and Celgard 2400 as separator.

Electrochemical measurements were performed in the potential range of 1.0 V to 3.0 V (versus $Li/Li^+$) at scan rate of 0.1 mV $s^{-1}$. Before cycling the cells, the $Li_2S$ cathodes were initially activated by charging up to 4.0 V at current rate of C/20. Electrochemical impedance spectroscopy (EIS) measurements were carried out using a frequency response analyzer in the frequency range of 0.01 Hz to 100 kHz with potentiostatic signal amplitude of 5 mV. The charge and discharge properties of the examined cathodes were measured galvanostatically (Kimiastat 126, Kimiapardaz Iran, Iran) at different currents (rates) in the range of 1.0 V to 3.0 V (versus $Li/Li^+$). All electrochemical tests were carried out at room temperature.

## RESULTS AND DISCUSSION

To characterize the synthesized LTO and Pr-LTO, their XRD patterns were studied, as shown in Fig. 1. The diffraction peaks conformed to cubic spinel structure in Joint Committee on Powder Diffraction Standards Joint Committee on Powder Diffraction Standards (JCPDS) card no. 49-0207, indicating that $Pr^{3+}$ ions were successfully introduced into the lattice of the spinel.

The relation between the interplanar spacing ($d$) and diffraction angle ($\theta$) can be expressed by the Bragg equation:

$$n\lambda = 2d\sin\theta, \quad (1)$$

where $\lambda$ is the x-ray wavelength.

According to the Bragg equation, the interplanar spacing is inversely proportional to the diffraction angle. The Bragg equation (Eq. 1) was applied to both LTO and Pr-LTO for several *hkl* lattice planes, namely (1 1 1), (3 1 1), (4 0 0), (3 3 0), and (4 4 0).

The XRD pattern shown in Fig. 2 reveals that the (1 1 1) peak of Pr-LTO shifted to smaller angle, indicating that the lattice parameter may be increased.

The results calculated for the (1 1 1) peaks of LTO and Pr-LTO were 8.288 Å and 8.313 Å, respectively. The larger lattice constant of Pr-LTO compared with LTO may be due to two reasons: (1) $Pr^{3+}$ (1.14 Å)[37] is larger in size than $Ti^{4+}$ (0.61 Å), so doping with Pr will increase the constant lattice of LTO; (2) doping of $Pr^{3+}$ at Ti sites will cause a certain amount of $Ti^{4+}$ to change to $Ti^{3+}$ for charge compensation,[38] leading to an increase in the lattice constant of LTO as $Ti^{3+}$ (0.67 Å) is larger than $Ti^{4+}$ (0.61 Å). Figure 3 shows SEM images of the LTO (a) and Pr-LTO (b) powders. Both powders exhibited a uniform particle size distribution, with average particle diameter of 50 nm.[30]

To provide further insight into the porous structure of the LTO and Pr-LTO nano/micro superstructures, BET measurements were performed. The BET specific surface area for LTO and Pr-LTO was 205.0 $m^2$ $g^{-1}$

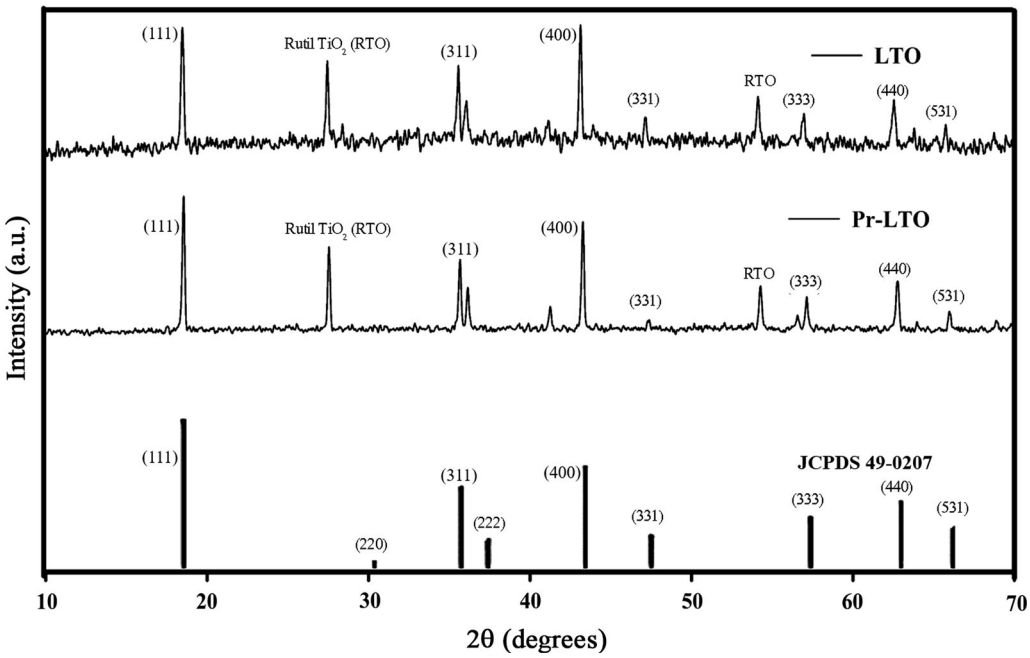


Fig. 1. XRD patterns of LTO and Pr-LTO.

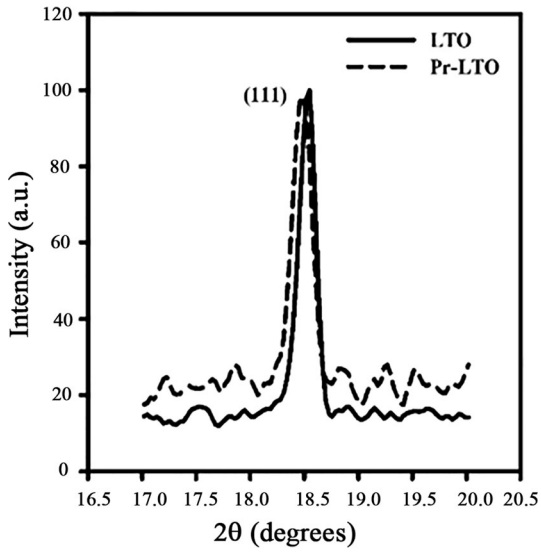


Fig. 2. Magnified (1 1 1) peaks of LTO and Pr-LTO.

and 319.1 $m^2 g^{-1}$, respectively. As shown in Fig. 4, the nitrogen adsorption–desorption isotherms could be attributed to type IVa, corresponding to capillary condensation accompanied by hysteresis, according to the International Union of Pure and Applied Chemistry (IUPAC) classification.[39]

Figure 5 shows the cyclic voltammograms (CV) of Pr-LTO. The curves show two peaks, one cathodic (at about 1.74 V versus $Li/Li^+$) and one anodic (at 2.05 V versus $Li/Li^+$), corresponding to the process of Li insertion into the spinel Pr-LTO and Li deintercalation from the spinel Pr-LTO, respectively. By comparison, Fig. 5 also shows the CV curve of LTO. It can be seen that the CV curves of LTO and Pr-LTO are similar. Because of the higher diffusivity of lithium ions and lower electrode polarization for Pr-LTO than LTO, the potential window (difference between the anodic and cathodic peaks) for Pr-LTO (310.0 mV) was much smaller than that of LTO (350.0 mV). Also, on doping with Pr, the kinetic characteristics of the LTO electrode were greatly improved and the pair of reversible redox peaks were enlarged and sharpened for Pr-LTO compared with pure LTO. These phenomena confirm that doping with Pr favored reversible intercalation and deintercalation of lithium ions.[30]

Figure 6 shows the cycling performance of LTO and Pr-LTO at rates of 0.5 C and 1 C. At 0.5 C, the 50th discharge capacity of Pr-LTO was 126 mAh $g^{-1}$, much higher than that (104 mAh $g^{-1}$) of LTO. The specific capacity retention of Pr-LTO and LTO during 50 cycles at 0.5 C was 94% and 80%, respectively, compared with the initial capacity in the first discharge cycle. At 1 C, the 50th discharge capacity of the Pr-LTO electrode was 96 mAh $g^{-1}$, whereas the corresponding value for LTO decreased to 66 mAh $g^{-1}$.

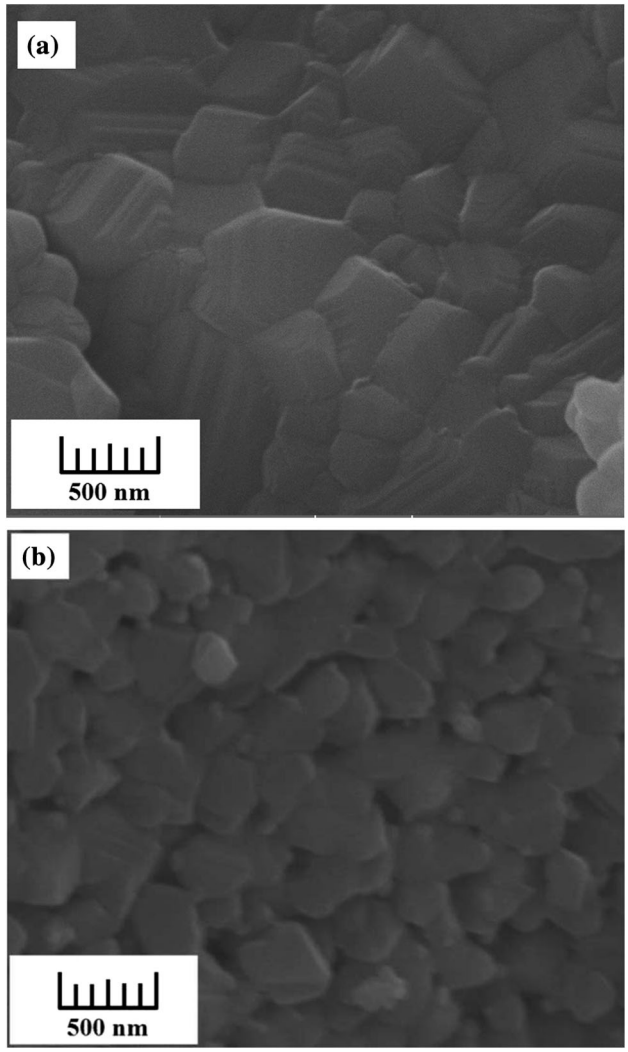


Fig. 3. SEM images of (a) LTO and (b) Pr-LTO.

In practical applications, lithium-sulfur batteries will be charged and discharged at low and high current density, respectively, and correspondingly, the anode could be charged and discharged in the same way. On doping $Pr^{3+}$ into LTO, the lattice volume of Pr-LTO expanded, and this phenomenon is useful for insertion and extraction of $Li^+$ ions.[30] As the charging current was increased, Pr-LTO showed excellent capacity retention. Even at 1 C, the charge capacity was 96 mAh $g^{-1}$, which is about 76% of the charge capacity at 0.5 C. According to these results, it can be deduced that Pr-LTO is a promising anode material with high rate capability and good cycling reversibility.

The initial discharge–charge curves of the LTO and Pr-LTO electrodes at different current rates from 0.05 C to 4 C are shown in Fig. 7. The discharge voltage plateau drops with increasing current rate for both electrodes. Despite the increase in current rate, a discharge plateau was not observed even at 2 C for either electrode. In the

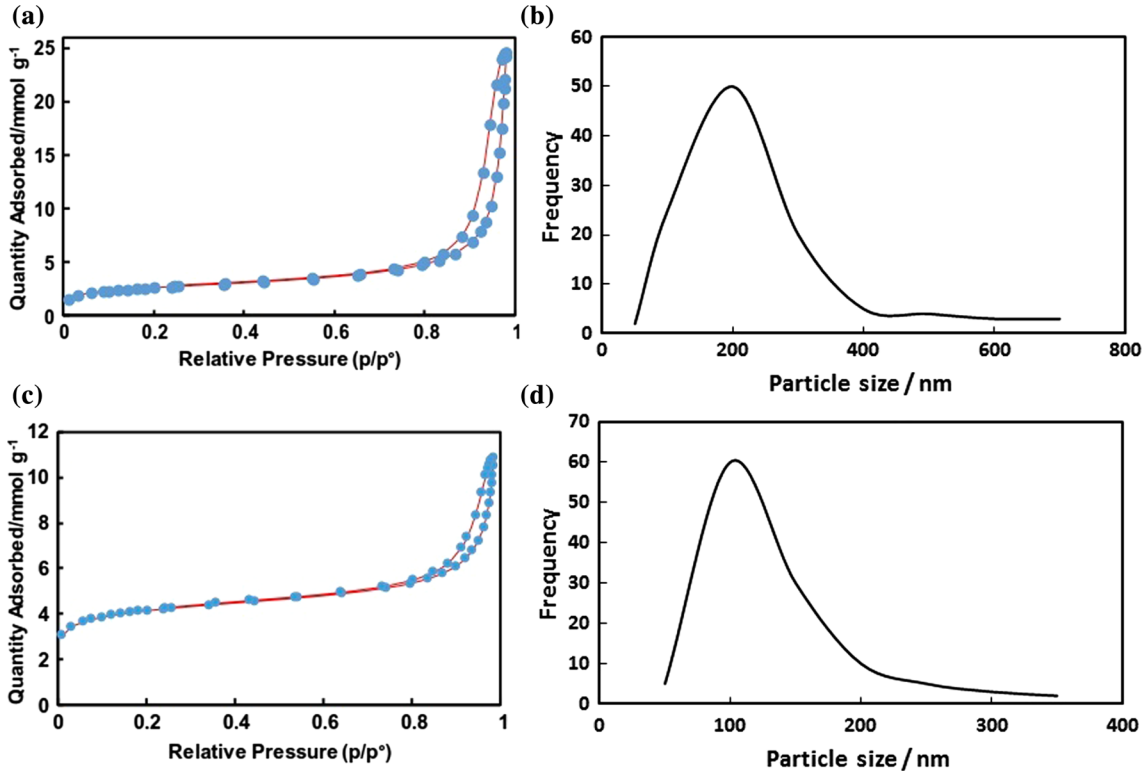


Fig. 4. Nitrogen adsorption–desorption isotherms (a, c) and size distribution (b, d) for synthesized LTO and Pr-LTO, respectively.

case of Pr-LTO, the discharge plateau lay at around 1.70 V at 0.05 C, while an evident discharge plateau could always be observed even when the current rate was 1 C. Meanwhile, the discharge and charge capacities decreased with increasing current rate. Compared with LTO, the Pr-LTO electrode exhibited excellent rate capability. At 0.05 C, Pr-LTO presented discharge capacity of 173 mAh $g^{-1}$, while LTO exhibited discharge capacity of only 158 mAh $g^{-1}$. The discharge capacity of Pr-LTO was slightly higher than the theoretical capacity of spinel LTO (175 mAh $g^{-1}$), which may be related to the nanocrystalline particles of carbon black used as electronic conductor during electrode preparation. At 4 C, the capacity of LTO was only 43 mAh $g^{-1}$; however, the discharge capacity of Pr-LTO remained at 52 mAh $g^{-1}$. This improvement in the high-rate capacity of Pr-LTO could be attributed to the enhanced electronic conductivity caused by the certain amount of Ti ions changed from $Ti^{4+}$ to $Ti^{3+}$.[30]

EIS plots for LTO and Pr-LTO are shown in Fig. 8. The EIS plots can be divided into high- and low-frequency regions, consisting of a semicircle and straight line, respectively. The intercept of the impedance with the $Z$ axis yields the ohmic resistance of the electrolyte. The semicircle in the high-frequency region represents migration of lithium ions at the electrode–electrolyte interface. Also, the straight line in the low-frequency region can be attributed to diffusion of lithium ions into the bulk

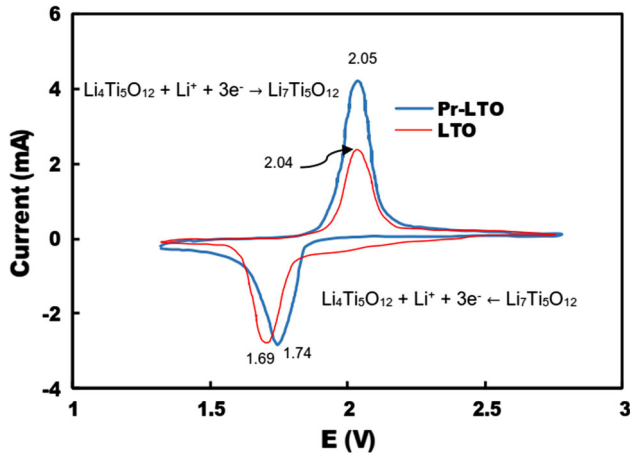


Fig. 5. Cyclic voltammograms of LTO and Pr-LTO obtained at scan rate of 0.1 mV $s^{-1}$.

of the electrode material, which is called Warburg diffusion. Fitting these EIS results using an equivalent circuit gives the ohmic resistance of the electrolyte ($R_s$), the charge-transfer resistance at the active material interface ($R_{ct}$), the double-layer capacitance, and the passivation film capacitance (CPE). $Z_w$ is the Warburg impedance caused by semiinfinite diffusion of $Li^+$ ions in the electrode.[30]

As seen in Fig. 8, the charge-transfer resistance of LTO (48.3 Ω) was dramatically decreased by Pr

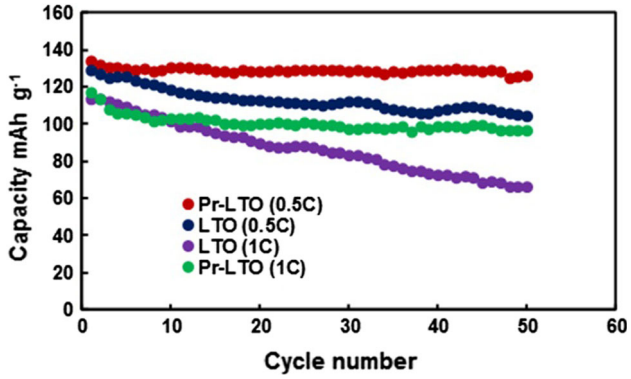


Fig. 6. Cycling profile of LTO and Pr-LTO at rate of 0.5 C and 1 C.

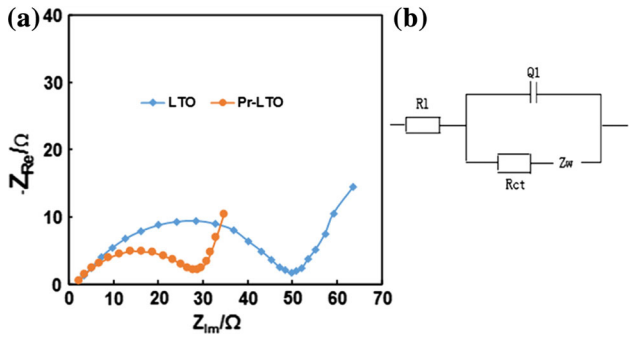


Fig. 8. (a) EIS Nyquist plots of experimental data and fitting results for LTO and Pr-LTO, (b) equivalent circuit for EIS data fitting.

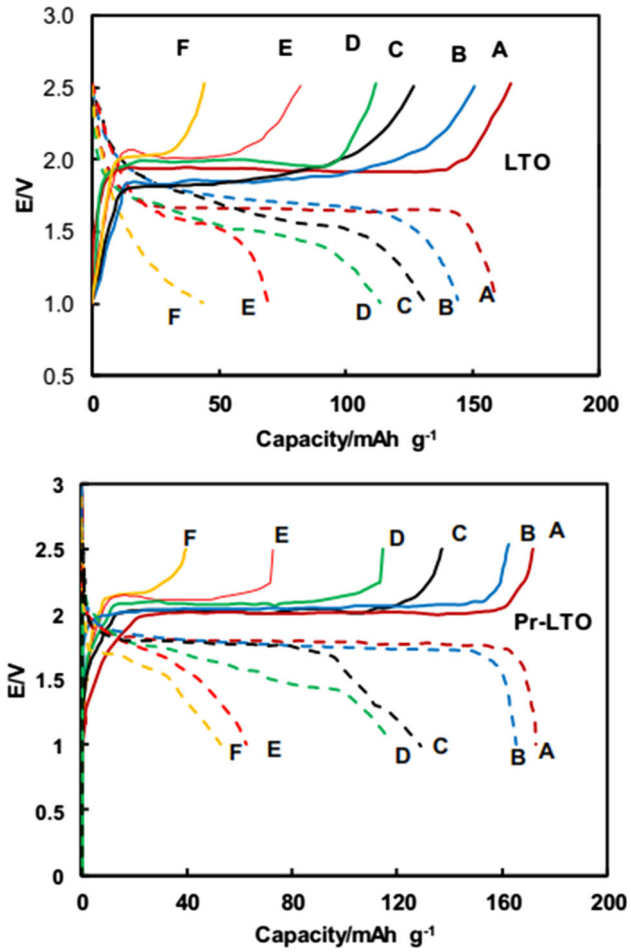


Fig. 7. Discharge–charge capacity performance and Coulombic efficiency of LTO and Pr-LTO electrodes at different current rates: (A) 0.05 C, (B) 0.1 C, (C) 0.5 C, (D) 1 C, (E) 2 C, and (F) 4 C, showing discharge (dotted line) and charge (dashed line) curves.

doping to 28.1 Ω in Pr-LTO, revealing improved surface electrochemical activity of the anode.

These EIS results and conductivity measurements demonstrate that the Pr-LTO electrode exhibited much higher conductivity than the LTO electrode. This confirms that Pr-LTO has potential as a high-rate anode material with higher electronic conductivity and lithium-ion diffusivity compared with LTO, indicating that Pr doping has positive effects on the reversible process of $Li^+$ intercalation and deintercalation.

## CONCLUSIONS

LTO and Pr-LTO powders were synthesized using a simple sol–gel method. XRD analysis proved that Pr-LTO possessed comparable crystallinity and appropriate phase purity with respect to LTO. Compared with the LTO electrode, the Pr-LTO electrode obtained using the same method exhibited higher capacity and better cycling efficiency. The capacity exhibited by Pr-LTO was 126 mAh $g^{-1}$ at 0.5 C and 96 mAh $g^{-1}$ at 1 C, even after 50 cycles. These results indicate that Pr-LTO could represent a promising material for anodes in Li-S batteries.

## CONFLICT OF INTEREST

The authors declare that they have no conflict of interest.

## REFERENCES

1. K. Amine, R. Kanno, and Y. Tzeng, *MRS Bull.* 39, 395 (2014).
2. L. Chen and L.L. Shaw, *J. Power Sources* 267, 770 (2014).
3. Z. Pourali, M.R. Sovizi, and M.R. Yaftian, *J. Alloys Compd.* 738, 130 (2018).
4. M.R. Sovizi and Z. Fahimi, *J. Taiwan Inst. Chem. E* 86, 270 (2018).
5. M.G. Kim and J. Cho, *Adv. Funct. Mater.* 19, 1497 (2009).
6. J.W. Long, B. Dunn, D.R. Rolison, and H.S. White, *Chem. Rev.* 104, 4463 (2004).
7. R. Cao, W. Xu, D. Lv, J. Xiao, and J.G. Zhang, *Adv. Energy Mater.* 5, 1402273 (2015).
8. G. Xu, B. Ding, J. Pan, P. Nie, L. Shen, and X. Zhang, *J. Mater. Chem. A* 2, 12662 (2014).
9. S.T. Seyyedin, M.R. Sovizi, and M.R. Yaftian, *Chem. Pap.* 70, 1590 (2016).
10. M.R. Sovizi and A.R. Madram, *Chem. Pap.* 71, 21 (2016).
11. S.T. Seyyedin, M.R. Yaftian, and M.R. Sovizi, *J. Solid State Electrochem.* 21, 649 (2016).
12. M.R. Sovizi, M.R. Yaftian, and S.T. Seyyedin, *New J. Chem.* 41, 12589 (2017).

13. G. Rong, X. Zhang, W. Zhao, Y. Qiu, M. Liu, F. Ye, Y. Xu, J. Chen, Y. Hou, and W. Li, *Adv. Mater.* 29, 1606187 (2017).
14. Y.M. Lee, N.-S. Choi, J.H. Park, and J.-K. Park, *J. Power Sources* 119, 964 (2003).
15. K.N. Wood, E. Kazyak, A.F. Chadwick, K.-H. Chen, J.-G. Zhang, K. Thornton, and N.P. Dasgupta, *ACS Cent. Sci.* 2, 790 (2016).
16. T. Osaka, T. Momma, Y. Matsumoto, and Y. Uchida, *J. Electrochem. Soc.* 144, 1709 (1997).
17. G. Zheng, S.W. Lee, Z. Liang, H.-W. Lee, K. Yan, H. Yao, H. Wang, W. Li, S. Chu, and Y. Cui, *Nat. Nanotechnol.* 9, 618 (2014).
18. R. Elazari, G. Salitra, G. Gershinsky, A. Garsuch, A. Panchenko, and D. Aurbach, *Electrochem. Commun.* 14, 21 (2012).
19. S. Goriparti, E. Miele, F. De Angelis, E. Di Fabrizio, R.P. Zaccaria, and C. Capiglia, *J. Power Sources* 257, 421 (2014).
20. J. Brückner, S. Thieme, F. Böttger-Hiller, I. Bauer, H.T. Grossmann, P. Strubel, H. Althues, S. Spange, and S. Kaskel, *Adv. Funct. Mater.* 24, 1284 (2014).
21. B. Duan, W. Wang, H. Zhao, A. Wang, M. Wang, K. Yuan, Z. Yu, and Y. Yang, *ECS Electrochem. Lett.* 2, A47 (2013).
22. X. Zhang, W. Wang, A. Wang, Y. Huang, K. Yuan, Z. Yu, J. Qiu, and Y. Yang, *J. Mater. Chem. A* 2, 11660 (2014).
23. C. Huang, J. Xiao, Y. Shao, J. Zheng, W.D. Bennett, D. Lu, L.V. Saraf, M. Engelhard, L. Ji, and J. Zhang, *Nat. Commun.* 5, 3015 (2014).
24. M. Reddy, G. Subba Rao, and B. Chowdari, *Chem. Rev.* 113, 5364 (2013).
25. M. Wagemaker, E.R. van Eck, A.P. Kentgens, and F.M. Mulder, *J. Phys. Chem. B* 113, 224 (2008).
26. T.-F. Yi, L.-J. Jiang, J. Shu, C.-B. Yue, R.-S. Zhu, and H.-B. Qiao, *J. Phys. Chem. Solids* 71, 1236 (2010).
27. Y. Wang, H. Li, P. He, E. Hosono, and H. Zhou, *Nanoscale* 2, 1294 (2010).
28. L. Qiao, X. Sun, Z. Yang, X. Wang, Q. Wang, and D. He, *Carbon* 54, 29 (2013).
29. Y. Wang, H. Rong, B. Li, L. Xing, X. Li, and W. Li, *J. Power Sources* 246, 213 (2014).
30. C. Lin, X. Fan, Y. Xin, F. Cheng, M.O. Lai, H. Zhou, and L. Lu, *J. Mater. Chem. A* 2, 9982 (2014).
31. K.-T. Kim, C.-Y. Yu, C.S. Yoon, S.-J. Kim, Y.-K. Sun, and S.-T. Myung, *Nano Energy* 12, 725 (2015).
32. C. Lin, M.O. Lai, L. Lu, H. Zhou, and Y. Xin, *J. Power Sources* 244, 272 (2013).
33. C. Chen, J. Vaughey, A. Jansen, D. Dees, A. Kahaian, T. Goacher, and M. Thackeray, *J. Electrochem. Soc.* 148, A102 (2001).
34. X. Li, M. Qu, and Z. Yu, *J. Alloys Compd.* 487, L12 (2009).
35. B. Tian, H. Xiang, L. Zhang, Z. Li, and H. Wang, *Electrochim. Acta* 55, 5453 (2010).
36. R.B. Khomane, A. Prakash, K. Ramesha, and M. Sathiya, *Mater. Res. Bull.* 46, 1139 (2011).
37. L. Suchow and M. Kokta, *J. Solid State Chem.* 5, 329 (1972).
38. Z. Zhong, *Electrochem. Solid State Lett.* 10, A267 (2007).
39. S. Lowell and J.E. Shields, *Powder Surface Area and Porosity* (Berlin: Springer, 2013).